https://doi.org/10.3311/PPch.44108

Periodica Polytechnica Chemical Engineering

Advancements in Selective Cellulose Acetate/Calcined Eggshell Membranes for Cr(VI) Effluent Treatment and Modeling Approach

Zohaib Atiq Khan[1,2], Sikander Rafiq*[1,3], Adeel Anwar[1,3], Ayesha Ajmal[1], Muhammad Zia Ul Haq[1], Asif Jamil[1], Tanveer Iqbal[1], Jibran Iqbal[4], Shafiq Uz Zaman[5], Shoaib Baber[1], Ali Ahmed[1]

[1] Department of Chemical, Polymer and Composite Materials Engineering, University of Engineering and Technology (UET) Lahore, New Campus (KSK), G.T. Road, Kala Shah Kaku, Sheikhupura 39021, Punjab, Pakistan
[2] Department of Chemical Engineering, University of Waterloo, 200 University Avenue West, Waterloo, Ontario N2L 3G1, Canada
[3] Department of Food Engineering and Biotechnology, University of Engineering and Technology (UET) Lahore, New Campus (KSK), G.T. Road, Kala Shah Kaku, Sheikhupura 39021, Punjab, Pakistan
[4] College of Natural and Health Sciences, Zayed University, P.O. Box 144534, Abu Dhabi, United Arab Emirates
[5] Department of Chemical Engineering, Ghulam Ishaq Khan Institute of Engineering Sciences and Technology (GIKI), Topi 23640, Swabi, Khyber Pakhtunkhwa, Pakistan
* Corresponding author, e-mail: sikander@uet.edu.pk

Received: 25 March 2026, Accepted: 22 June 2026, Published online: 25 September 2026

Abstract

Mixed matrix membranes (MMMs) are a promising approach for hexavalent chromium Cr(VI) removal from wastewater. In this study, asymmetric membranes were synthesized by incorporating calcined eggshell as a bio-fillers in a polymer matrix. MMMs were synthesized via phase inversion technique at various filler loadings ranging from 5–20% wt.%. Characterizations of synthesised membranes were performed using scanning electron microscopy, thermogravimetric analysis and permeability studies. The results showing the highest flux of 3503 ± 32 L m^{-2} h^{-1} and 60.5 ± 0.8% Cr(VI) rejection were obtained by a membrane with 20 wt.% filler loading. Modeling approach was conducted to compare the experimental data with the pore network and continuum models to predict the transport properties. The pore network model showed the most accurate prediction of membrane transport behavior, with an average absolute relative error of 15.03% compared to other continuum models. The study thus provided the impact of structural influences on pressure distribution within membranes, emphasizing the need of including pore size distribution in the analysis.

Keywords

mixed matrix membranes, calcined eggshell, hexavalent chrome, permeation flux, pore network modeling

1 Introduction

The utilization of membrane technology for water treatment has been extensively employed for the purpose of generating potable water, recuperating reusable constituents, or refining industrial effluents [1–3]. The technology in question has garnered significant interest in recent times owing to its multifaceted processing capabilities, superior removal efficiency, eco-friendliness, reduced pollution levels, simplified operational procedures, minimal maintenance requirements, easy scalability, superior performance and economically viable nature when compared to conventional separation methods [4–7]. The primary focus of current research is the improvement and development of existing membranes through advancements and upgrades in membrane materials, with the aim of achieving enhanced efficiency and performance [8–13]. Mixed matrix membranes (MMMs) have emerged as a promising approach to tackle the aforementioned factors due to their superior performance, fouling resistance, permeate quality, and durability [14, 15]. MMMs referred as heterogeneous membranes, are composed of a continuous polymer matrix with dispersed porous molecular materials as fillers [16–19]. The immersion precipitation method is a widely recognized approach for producing asymmetric membranes [20–24]. According to Tian et al., cellulose acetate (CA) is commonly used material to synthesis nanofiltration and reverse osmosis membranes [25–27]. This polymer is noteworthy due to its attractive properties such as biodegradability, environmental stability,

Cite this article as: Khan, Z. A., Sikander Rafiq, S., Anwar, A., Ajmal, A., Haq, M. Z. U., Jamil, A., Iqbal, T., Iqbal, J., Zaman, S. U., Baber, S., Ahmed, A. "Advancements in Selective Cellulose Acetate/Calcined Egg-shell Membranes for Cr(VI) Effluent Treatment and Modeling Approach", Periodica Polytechnica Chemical Engineering, 2026. https://doi.org/10.3311/PPch.44108

cost-effectiveness and commercial availability [28–31]. In addition, CA is derived from renewable sources and recognized for its favorable mechanical properties, hydrophilic nature and transport properties [28, 32–35].

In the development of MMMs, the selection of suitable filler is quite challenging issue due to the textural characteristics, compatibility and interaction with polymer matrix [16, 36–38]. One of the most practical approach is to improve the performance of the membranes by the inclusion of inorganic material like bio-fillers in the polymeric matrix. The integration of inorganic materials has been investigated as a means of enhancing various properties such as flux, antifouling capability, and thermal and mechanical properties [33, 39–41]. The utilization of bio-fillers sourced from natural raw materials is being extensively explored as a viable alternative to the prevalent inorganic fillers due to their cost-effective solutions. The utilization of waste materials and environmentally sustainable nature have spurred further advancements in the production of MMMs. The eggshells have been extensively examined as a common bio-filler in numerous studies [42–44]. The disposal of eggshells, a solid waste primarily generated by the food industry and households, can pose significant challenges, including potential risks to public health, contamination of water sources and environmental pollution. According to Lumlong et al. and Habte et al., a significant rise of approximately 44% in food waste was observed from 2005 to 2025 [45, 46]. The utilization of waste materials as a precursor for the synthesis of composites has been identified as a cost-effective, environmentally friendly and sustainable approach [17, 45, 47, 48]. Park et al. observed 99% removal of Cr by using calcined eggshells as a bio adsorbent [49]. Lovey et al. synthesized polysulfone-based membranes using the phase inversion technique. Chromium rejection and the flux of the pristine membrane, using crossflow filtration unit, are found to be 64% and 44 L m^{-2} h^{-1}, respectively [50]. Li et al. developed CA/polyaniline (PANI) composite membrane, that was doped by phytic acid (PA), and the maximum adsorption capacities for Cr(VI) achieved is 94.34 mg g^{-1} [51]. Previous studies used eggshells for heavy metal removal in a membrane bioreactor system that proved to be efficient green adsorbent. The porosity and surface characteristics of eggshell membrane rendered an effective bio-adsorbent, capable of extracting heavy metals, phenolic compounds, dyes, and pesticides from wastewater [52, 53].

Past studies extensively utilized modeling techniques in MMMs as a powerful tool for validation by employing various membrane models [4, 54–56]. They provide reliability for membrane evaluation, providing valuable insights regarding various factors that affect the performance of membranes [56–58].

Pore network modeling (PNM) has gained significant attention in recent years due to its ability to predict the transport properties of porous media. It is a powerful tool for simulating fluid flow, transport and mechanical properties of porous materials at a pore scale. Several studies have demonstrated the effectiveness of pore network modeling in understanding the complex fluid-solid interactions that occur within porous materials [59, 60]. For example, research has been done on the use of pore network modeling in the development of catalysts, oil recovery and modeling energy storage devices [61–64]. The latest research in pore network modeling includes work done on the optimization of porous media structures for flow enhancement and modeling of shale gas flow [65]. These studies have shown that pore network modeling is an important tool for predicting the transport properties of porous materials, therefore the technique can be effectively utilized to study transport in MMMs as they represent perfect porous structure. Moreover, as per authors' knowledge, PNM technique is not utilized in MMMs although it has significant potential in the field of membrane science.

The current study focused on the synthesis of asymmetric cellulose acetate (CA)/calcined eggshell (CES) membranes via immersion precipitation for wastewater treatment. Several characterizations of MMMs were performed at varying CES filler loadings for evaluating the morphological, thermal and permeation properties of synthesized membranes. The experimental findings were evaluated utilizing pore network and continuum modeling novel strategy, not previously used, in MMMs for Cr(VI) removal.

2 Experimental section

2.1 Materials and methods

The CA beads with an acetyl content 53.5–54.5% (molecular·mass 52,000 g mol^{-1}) and the solvent, 1-methyl-2-pyrrolidinone (NMP) (99.0% analytical purity, boiling point 202, density 1030 kg m^{-3}) was supplied by Sigma-Aldrich. Eggshells obtained from a local bakery were modified and utilized as an inorganic filler as per the process shown in Fig. 1(a). Cr(VI) stock solution of 1000 mg L^{-1} was prepared by dissolving 2.83 g of potassium dichromate in 1 L of distilled water. 200 mg L^{-1} working solution was prepared by diluting 200 mL of the stock solution to a final volume of 1 L using distilled water.

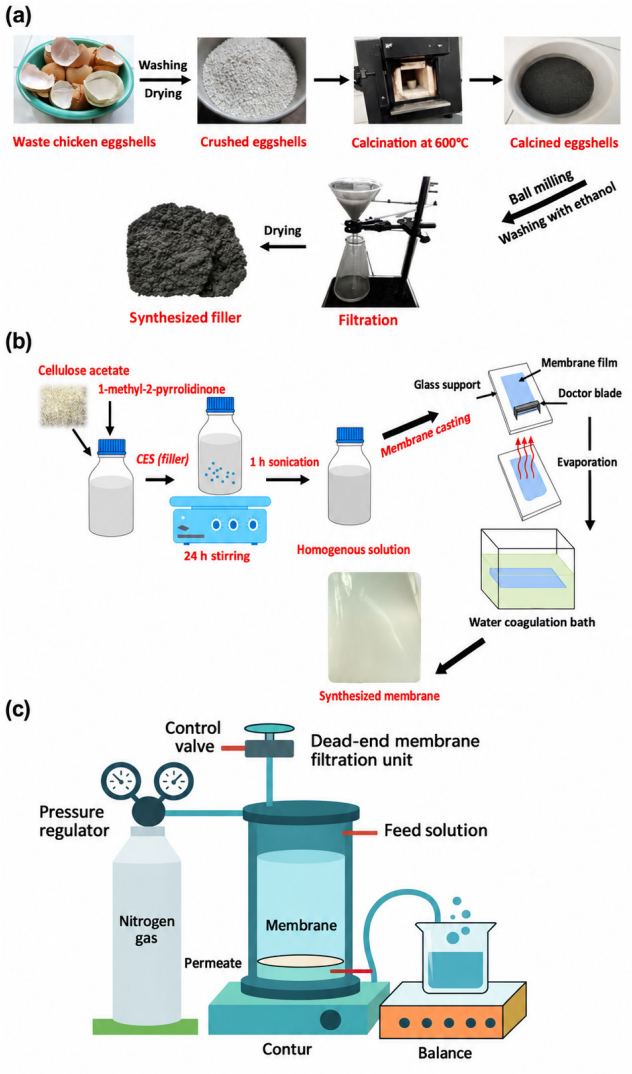

Fig. 1 Synthesis of (a) CES bio fillers, (b) asymmetric MMMs, (c) dead-end filtration unit

2.2 Preparation of calcined eggshell bio-derived inorganic filler

Chicken eggshells were cleaned several times with tap water to remove impurities and interfering material like organics and salts, followed by three rinses with deionized water. The sample was then placed in an oven and dried at 100 °C for 12 h. The dried sample was crushed followed by calcination process in a muffle furnace at 600 °C at 4 h. The fraction with a particle size < 60 µm was obtained through ball milling and sieving *via* a vibrating sieve shaker. The sample was rinsed three times with ethanol to eliminate contaminants prior to filtration. The obtained fraction accounted for 65% of the total dried sample. After drying the sample at 78 °C for 2 h, grayish colored CES filler in powdered form was finally obtained (Fig. 1(a)).

2.3 Synthesis of asymmetric mixed matrix membranes

A dope solution containing 15 wt.% CA was prepared by dissolving the polymer in the NMP solvent. The impact of CES on membrane morphology was examined by adjusting the filler loading between 5–20 wt.% in the dope solution. The homogenous mixture was obtained by stirring the dope solution for 24 h at 700 rpm and 25 °C, using a teflon-lined magnetic stirrer in a borosilicate glass bottle. It was followed by sonication process for 45 min to ensure the homogenous dispersion of the particles. The dope solution was also agitated to eliminate air bubbles and was left undisturbed for an hour at room temperature. The prepared dope solution was poured on the clear glass surface for membrane casting using an adjustable Elcometer casting knife (Elcometer Instruments Ltd., Manchester, UK) set to 200 µm, to ensure uniform membrane development. The membrane was kept at ambient conditions (25 °C, relative humidity ~50%) for 30 s to allow partial solvent evaporation. It was followed by coagulation process by immersion into distilled water bath. In the phase inversion technique used in this study, the precipitation of the membrane film was induced by solvent exchange in a non-solvent (distilled water) precipitation bath. The developed flat sheet membrane was subsequently immersed in a separate container filled with fresh distilled water, in order to eliminate any residual NMP. The membrane was ready for testing after 24 h (Fig. 1(b)).

3 Characterizations

3.1 Scanning electron microscopy and thermogravimetric analysis

Morphological studies of the synthesized MMMs were carried out using a scanning electron microscope (VEGA3 TESCAN, TESCAN ORSAY HOLDING, Brno, Czech Republic), to attain qualitative information for the respective surfaces and cross-sections in terms of thickness and microstructures. For cross sections, membranes were fractured in liquid nitrogen. Thermal stability of the different compositions of MMMs were analyzed by using thermogravimetric analyzer (PerkinElmer TGA 4000, PerkinElmer Inc., Waltham, MA, USA). The TGA profile of CES was analyzed at a heating rate of 10 °C min^{-1} up to 900 °C under a nitrogen atmosphere. Subsequently, the degradation of various compositions of MMMs was evaluated using a three-stage decomposition analysis protocol consisting of moisture evaporation, polymer chain degradation, and decomposition of residual organic constituents at a constant heating rate of 10 °C min^{-1}.

3.2 Permeation flux and solute rejection performance

The study employed a stainless-steel dead-end filtration unit (Sterlitech Corporation, Kent, WA, USA) to conduct the filtration experiments (Fig. 1(c)), having membrane effective area of 1.2×10^{-3} m^2. 100 mL feed solution was subjected to nitrogen gas at a predetermined pressure as it passed through the cell. The permeate sample was obtained *via* atmospheric pressure. The feed solution was agitated at 700 rpm using a teflon-coated magnetic stirrer. A 200 mg L^{-1} Cr(VI) solution was used as the feed. For conducting the experiments, feed pressure was maintained at 2 bar at ambient conditions (25 °C, relative humidity ~50%). The volumetric flow rate and residence time of the feed stream that passed through the membrane at steady state were recorded.

The permeation flux for each membrane was calculated from Eq. (1) [8]:

$$J = \frac{Q}{A \times t}, \tag{1}$$

where J, Q, A and t represents the permeate flux, volumetric flow rate of the permeate, membrane area and filtration time, respectively. The Cr (VI) salt rejection R from the membrane was determined by Eq. (2):

$$R = \left(1 - \frac{C_p}{C_f}\right) \times 100, \tag{2}$$

where C_f and C_p are the solute concentrations in the feed and permeate, respectively [66]. The minimization of experimental error was achieved by conducting a minimum of five measurements for each type of membrane at steady state.

The values reported in Table 1 represent the average of at least five independent measurements conducted under steady-state conditions, and the associated deviations correspond to the standard deviation of the experimental data. The membrane thickness and the mean pore size were determined from SEM image analysis using ImageJ software, whereas the conductivity and the pH were measured using a digital conductivity meter (HI98192, Hanna Instruments, Woonsocket, RI, USA) and a pH meter (HI2211, Hanna Instruments, Woonsocket, RI, USA), respectively. The permeation flux and the Cr(VI) rejection were obtained from dead-end filtration experiments performed at 2 bar and 25 °C.

4 Modeling mixed matrix membranes

A reliable modeling approach can accurately be utilized to forecast the performance of the membranes and optimize the process thereby reducing cost and time. The performance evaluation typically involves two key aspects: predictions of flux and rejection. These are generally conducted in membrane process, employing a range of models and theories to understand the underlying transport mechanisms. The transport mechanism determines how membrane performance is modeled in water treatment. Earlier studies have used several permeation models based on analogies.

This study investigates the performance of the synthesized membranes using two different modeling techniques, namely pore network model and continuum model. The subsequent section provides a detailed explanation of the methodology adopted in both modeling techniques. The comparative analysis and accuracy of each method are discussed in Section 5.

4.1 Pore network model development

This study focused on developing a porous network model to simulate the behavior of MMMs under different filler loadings and its effects on transport properties. Further, the performance of different modeling techniques was compared with the obtained experimental data.

The porous networks were generated using the open-source Python package OpenPNM [67]. The physical properties of all the porous structures used in the model are listed in Table 1. The pore network was constructed as a regular cubic lattice in OpenPNM, where each internal pore is connected to six nearest neighbors (coordination number = 6). The topology was kept uniform, while the geometrical properties of the network including pore diameter, throat size and membrane thickness

Table 1 Evaluation of membrane performance through permeation flux and solute rejection

Membrane type*	Thickness (μm)	Mean pore size (μm)	Conductivity (μS)	pH	Permeation flux (L m^{-2} h^{-1})	Rejection (%)
CA-0	200 ± 11	0.360 ± 0.028	321	3.8	2741 ± 83	32 ± 0.2
CA-5	226 ± 13	0.410 ± 0.035	303	3.9	2940 ± 70	36 ± 0.6
CA-10	271 ± 15	0.243 ± 0.021	181	4.2	3397 ± 67	59.5 ± 0.9
CA-15	267 ± 13	0.214 ± 0.018	171	4.3	3318 ± 15	59.5 ± 0.5
CA-20	274 ± 12	0.133 ± 0.012	156	6.1	3503 ± 32	60.5 ± 0.8

* The membrane samples were designated as CA-0, CA-5, CA-10, CA-15, and CA-20, representing cellulose acetate membranes incorporated with 0, 5, 10, 15, and 20 wt.% calcined eggshell filler loadings, respectively.

were assigned based on SEM-derived experimental data (mean pore size and membrane thickness). This approach enabled the incorporation of realistic structural characteristics while maintaining a simplified and tractable network representation. The generated porous networks are shown in Fig. 2. In Fig. 2(a), the thickness of each membrane is plotted along the *x*-axis, while the *y*-axis and *z*-axis represent the area of the membrane in two-dimensional space. This enabled a distinct visualization of the porous network structure. It indicated the influence of various properties like pore size and connectivity, on transport characteristics of the mixed matrix membranes.

To quantify the flux across the porous network, mass conservation was applied to each individual pore using Eq. (3), where q_{ij} represents the volumetric flow rate between connected pores *i* and *j*:

$$q_{ij} = \sum_{j=1}^{n} \times g_{h,ij} \times \left(P_j - P_i\right) = 0 \tag{3}$$

In the simulation, each pore is identified by an index *i*, and its neighboring pore with index *j*, while the number of

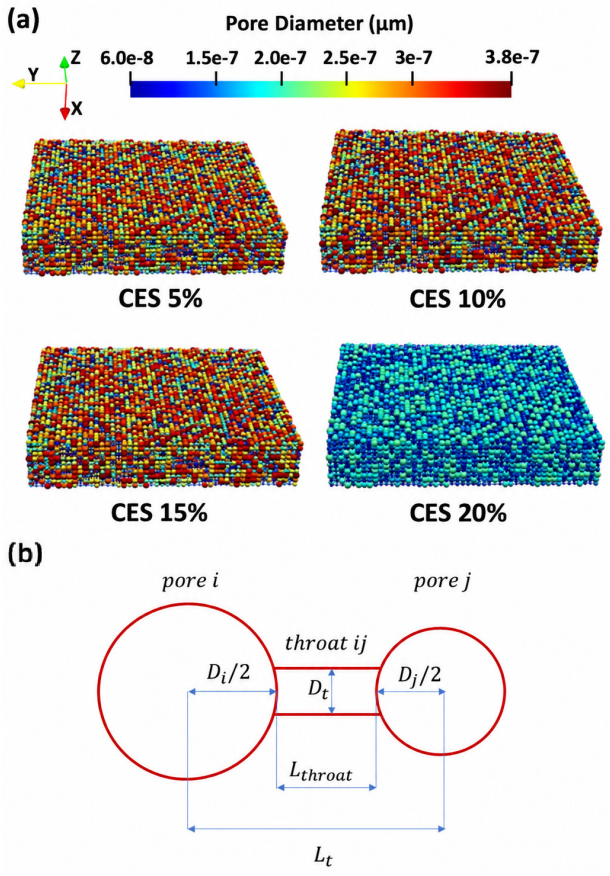

Fig. 2 (a) Pore networks of MMMs with different loading. (b) Pore-throat-pore assembly definition in the pore network model (where D_i and D_j are the diameters of pore *i* and pore *j*; $D_i/2$ and $D_j/2$ are the pore radii; D_t and L_{throat} are the diameter and length of the pore throat; and L_t is the total center-to-center length between pore *i* and pore *j*).

neighboring pores is denoted by *n*. The net flow through pore *i* is represented by q_i. $g_{h,ij}$ represents the hydraulic conductivity of the flow between pore *i* and pore *j*. The pressure in the respective pores is represented by P_i and P_j. The length and diameter of pores and throats are major factors influencing hydraulic conductivity as represented in Eq. (4).

$$g_{h,N} = \frac{\pi \times D_N^4}{128 \times \mu L_N}, \quad N \in \left\{P_i, \quad P_j, \quad \text{throat}\right\}, \tag{4}$$

where D_N and L_N are the diameter and length of each individual conduit segment *N*, representing the throat *ij* (diameter D_t, length L_{throat}) and the half-pores P_i and P_j (defined as the conduit segments extending from each pore sphere's center to the throat junction, with diameters D_i, D_j and effective lengths equal to their pore radii $D_i/2$ and $D_j/2$, as depicted in Fig. 2(b)), and μ denotes the dynamic fluid viscosity. The study used Eq. (4) to determine the hydraulic conductivity for individual sections. Finally, the net conductivity for the pore-throat-pore assembly $g_{h,ij}$ was evaluated using the linear resistor series theory using Eq. (5) [59].

$$\frac{1}{g_{h,ij}} = \frac{1}{g_{h,Pi}} + \frac{1}{g_{h,t}} + \frac{1}{g_{h,Pj}}, \tag{5}$$

where $g_{h,Pi}$ and $g_{h,Pj}$ represent the hydraulic conductivities of the half-sections of pore *i* and pore *j*, respectively, while $g_{h,t}$ denotes the hydraulic conductivity of the throat connecting them. To calculate the total flow rate $\dot{q}$ across the network, Eq. (3) was applied to each pore in the network, which resulted in a system of linear equations. The pressures at the boundaries were defined on both faces perpendicular to the *x*-axis of the network, which were utilized to solve these equations. Dirichlet pressure boundary conditions were applied along the *x* direction, where the inlet pressure was fixed at 2 bar (corresponding to the experimental feed pressure) and the outlet pressure was set to 1 bar (atmospheric pressure). All other faces of the network were treated as no-flow (Neumann) boundaries, ensuring one-dimensional transport across the membrane. Once $\dot{q}$ was determined, *J* was calculated using the following expression:

$$J = \frac{\dot{q}}{A} \tag{6}$$

For fluid flow in the *z* direction, the area of the pore network *A* perpendicular to the direction of flow was calculated by ZYL_C^2, where *Y* and *Z* referred to the number of pores in the respective dimensions of the network, while L_C is the lattice constant (the distance of one pore-throat-pore assembly).

4.2 Continuum model development

In continuum-based modeling approach, models based upon osmotic pressure model, Hagen–Poiseuille and Carman–Kozeny equations were considered [68].

Genne et al. [69] proposed a model based on the Hagen–Poiseuille equation to describe the flow through pores of a membrane. This model relates the membrane permeability to its porosity, mean pore diameter, and membrane thickness. However, Li et al. highlighted that the transport mechanism in porous membranes were more complex and dependent on various membrane properties such as pore size, pore distribution, porosity, and pore geometry [70, 71].

To account for these characteristics, the Hagen-Poiseuille equation was modified by incorporating the porosity and tortuosity of the pores. The resulting Eq. (7) accounted for the flux through the membrane in terms of water viscosity, applied pressure ΔP, pore size D, membrane porosity ε, and membrane thickness L [68].

$$J = \frac{\varepsilon \times D^2}{32 \times \eta} \times \frac{\Delta P}{L} \tag{7}$$

The membrane porosity and tortuosity τ were evaluated using the Smolders–Franken and Mackie–Meares correlations, as expressed in Eqs. (8) and (9), respectively [72]. Where ρ_m and ρ_{pool} are the densities of the membrane and the polymer material, respectively.

$$\varepsilon = 1 - \frac{\rho_m}{\rho_{pol}} \tag{8}$$

$$\tau = \frac{\left(2 - \varepsilon\right)^2}{\varepsilon} \tag{9}$$

When analyzing porous membranes, it is important to recognize that the pores may not always have a cylindrical or linear geometry. Therefore, an alternative approach was assumed that the membrane consisted a collection of roughly spherical particles. In such cases, the Carman–Kozeny equation was utilized to calculate the flux through the membrane [68, 73]:

$$J = \frac{\varepsilon^3}{K \times \eta \times S^2 \times \left(1 - \varepsilon\right)^2} \times \frac{\Delta P}{L}, \tag{10}$$

where S is the specific surface area (m^2/m^3), K is a Carman–Kozeny constant (dependent on the shape of the pores and tortuosity).

Both aforementioned models are theoretical equations, based on idealized assumptions. The actual structure of the membranes diverged from these assumptions. The osmotic pressure model was commonly used to describe the permeation flux, as expressed in Eq. (11) [68, 73]:

$$J = \frac{\Delta P}{\eta_p \times \left(R_m + R_{tot}\right)}, \tag{11}$$

where η_p is the dynamic viscosity of the permeate, R_m represents the intrinsic membrane resistance, and R_{tot} denotes the total filtration resistance.

The intrinsic membrane resistance could be determined by applying the Hagen–Poiseuille law Eq. (7) with porosity, correction factor μL (dimensionless), which describes the meandering of actual pores inside the membrane (typically 1×10^{-23} used), the thickness of the membrane and the particle diameter.

$$R_m = \frac{9}{4} \times \frac{\left(1 - \varepsilon\right)^2}{\varepsilon^3} \times \frac{\mu L \times L}{D^2} \tag{12}$$

The total filtration resistance (R_{tot}) was calculated according to Darcy's law (Eq. (13)) with the permeate viscosity η_P (Pa·s) and the permeate flux J_p:

$$R_{tot} = \frac{\Delta P}{\eta_P \times J_P} \tag{13}$$

To enhance the accuracy of the membrane performance prediction, it was imperative to account for the fouling effect during the treatment of actual water samples that contained foulants. Fouling resistance ($R_{foul} = R_{tot} - R_m$) was thus included in Eq. (13). The present model was recognized as the hydraulic model of filtration resistance, referred as the resistance in series model, in academic research.

As shown in Eqs. (14) and (15), the average absolute relative error (AARE%) was used to determine the discrepancy between the predicted and experimental values.

$$\text{ARE}_i = \frac{J_i^{cal} - J_i^{\exp}}{J_i^{\exp}} \tag{14}$$

$$\text{AARE\%} = \frac{100 \sum_{i=1}^{d_j} \text{ARE}_i}{d_j}, \tag{15}$$

where ARE_i is the absolute relative error for data point i, while J_i^{cal} and J_i^{exp} are the theoretically derived and experimentally determined values of the relative permeation flux of the solution, respectively. i represents the index of a given data point and d_i is the total number of data points.

5 Results and discussion

5.1 Thermal analysis

The thermal stability of the sample was assessed using TGA analysis. The corresponding TGA and derivative thermogravimetric (DTG) curves are presented in Figs. 3(a) and 3(b), respectively, at a heating rate of 10 °C min^{-1}, with their corresponding derivatives. The degradation of all the synthesized membranes occurred in three steps. The initial mass loss (from 50 °C and 270 °C) was primarily attributed to the evaporation of physically adsorbed moisture and the release of low-molecular-mass volatile compounds. The second phase (from 270 °C to 395 °C), represented the depolymerization of the polymeric chains. The third step (from 395 °C onwards) represented the thermal decomposition of the remaining organic constituents, leaving behind inorganic residual matter. Interestingly, distinctive trends were observed particularly after 270 °C, where the mass loss was reduced with the increase in filler loadings in the CA matrix. The mass loss ranged from 69.2%, 69.1%, 65.4%, 63.1%, and 60.5% from 0 to 20 wt.% filler loadings, respectively. The inclusion of CES filler in polymer matrix indicated improvement in thermal stability of the synthesized membranes, which is consistent with previous research [74, 75].

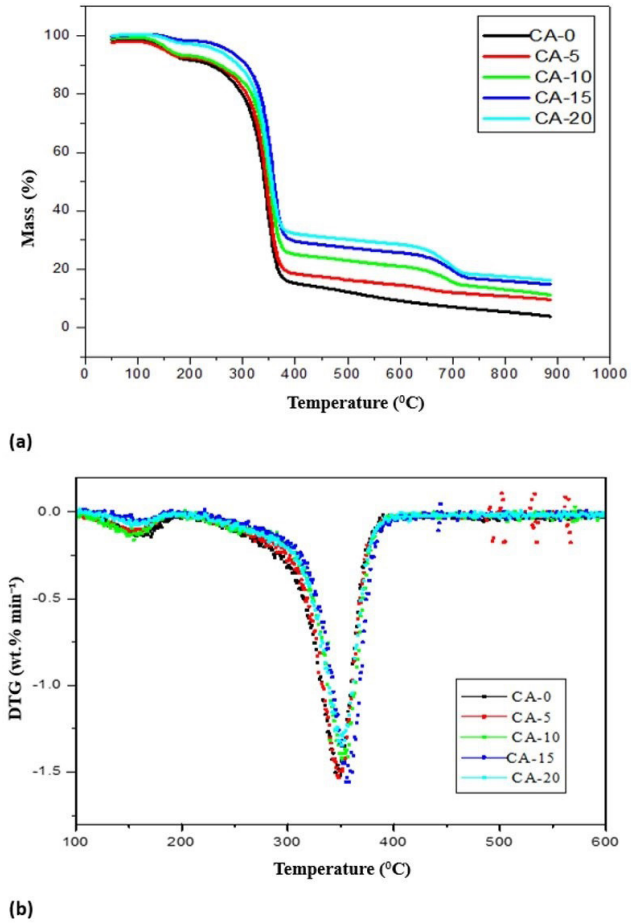

Fig. 3 CA/CES membranes (a) TGA profiles (b) DTG profiles

5.2 Morphological characterization

The membranes exhibited an asymmetric structure with thin dense top skin layer indicating a selective barrier (Fig. 4(a)). It is supported by a thicker porous sublayer with a finger-like macrovoid structure (known as the support layer) (Fig. 4(b)). The presence of the porous sub-layer contributes to the mechanical robustness of the material, while the skin layer exhibits a relatively thin and dense structure, leading to relatively high resistance and low flux [76]. The synthesized MMMs possess an increased porosity as compared to pure polymeric membranes. This can be due to the presence of uniformly distributed fillers leading to channeling in the top skin layer of the matrix, thus creating stronger pore interconnected networks with increase in filler loading. During the phase inversion process the quantity of the solvent decreased while the polymer concentration remained constant, thus the solution became more viscous, which prevented the membrane from swelling and consequently affected the MMMs thicknesses. CES particles inhibit the proximity of polymer chains, thereby producing free volume [77].

5.3 Permeation analysis

As shown in Table 1, the permeation flux increased from 2741 ± 83 to 3503 ± 32 L m^{-2} h^{-1} with increasing CES filler loading (5–20 wt.%), indicating enhanced membrane permeability. These findings pointed towards an increase in the flux across MMMs as compared to the pure CA membrane due to the hydrophilic nature of the inorganic CES fillers. The observed increase in the permeation flux of the modified membrane can be attributed to several factors including the enlargement of the pores size, the enhancement of the surface hydrophilicity, and an increase in the effective filtration area. The membrane exhibited a porous surface that possessed a favorable inner structure, thereby conferring a distinct advantage. The synergistic impact of the greater porosity, enhanced pore connectivity and augmented effective free volume promotes more efficient water transport, resulting in a superior permeation flux relative to the unmodified membrane. The permeation flux at 20 wt.% filler loading was observed to reach its highest value of 3503 ± 32 L m^{-2} h^{-1} among the other synthesized CA membranes. This value represented an increase of approximately 27.8% compared to the intrinsic

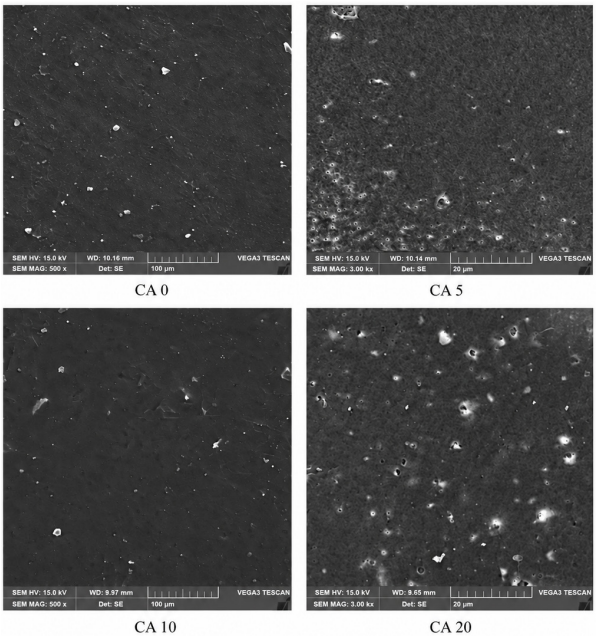

(a)

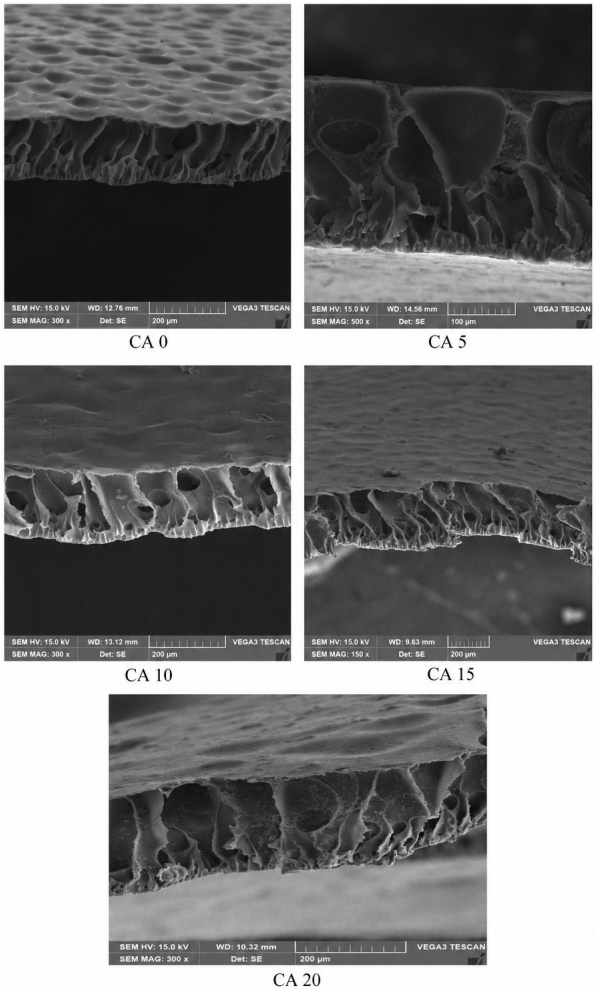

(b)

Fig. 4 SEM images of (a) surfaces (b) cross-sections of the CA/CES membranes

membrane with permeation flux of 2741 ± 83 L m^{-2} h^{-1}. The high permeation fluxes are ascribed to the porous structures of the membranes under low operating pressure.

The incorporation of bio-derived CES filler enhanced the Cr(VI) removal performance of the membranes, as evidenced by the increase in rejection from 32 ± 0.2% for pristine CA membrane to 60.5 ± 0.8% for CA-20 membrane (Table 1). The improved rejection behavior may be attributed to the interaction of Cr(VI) ions with the CES-containing membrane structure and the increased availability of the active sites at higher filler loadings. The incorporation of CES fillers into the membranes facilitated Cr(VI) ion removal in acidic conditions *via* surface adsorption while simultaneously demonstrating a commendable neutralization capacity. The amount of Cr(VI) removed from the aqueous solution showed a linear increase as the dosage of calcined eggshell was raised. Maximum rejection of 60.5 ± 0.8% was observed for 20 wt.% CES MMM as a result of the highest sorption sites for Cr(VI) uptake. The remaining three MMMS showed rejected rate in the following order: CA/CES 15% > CA/CES 10% > CA/CES 5%. Consequently, for the CA-20 membrane, the Cr(VI) concentration was reduced from 200 mg L^{-1} in the feed solution to 79 mg L^{-1} in the permeate stream. By including a membrane system with these sorbents, fouling can be mitigated [49]. The findings of this study are consistent with prior research, which suggests that the incorporation of filler particles can enhance the permeation flux [39]. The moderate rejection rates achieved are ascribed to the comparatively greater pore size of the CA/CES membranes, rendering size exclusion, inadequate for the complete removal of Cr(VI) species. Moreover, the transport is regulated by a synergy of convective flow and diffusion, facilitating the selective passage of ions. The restricted surface charge of the membrane diminished the electrostatic repulsion towards the negatively charged chromate moieties. At higher filler loadings, the enhanced pore connection increased the permeability but restricted further advancements in rejection, leading to a plateau effect. Table 2 contextualizes this work within existing literature [50, 78, 79]. Membranes with comparable porosity architectures demonstrate modest rejection rates, while nanofiltration and reverse osmosis systems, characterized by dense selective layers and robust electrostatic contacts, produce markedly greater rejection rates.

5.4 Comparison of modeling approaches

Table 3 presents a comparative analysis of the results obtained from pore network models, continuum models

Table 2 Performance of previously reported mixed matrix membranes for Cr(VI) removal*

MMMs (different filler loadings)	Rejection (%) range	Ref.
CA/CES (0–20 wt.%)	32–60.5	Present study
Oxidized MWCNT/PSf Azide/Amide/ MWCNT/PSf Pristine PSf	~ 33-86 ~ 80-94 ~10	[78]
PSf/MMT PSf/mMMT	~ 71-89 ~ 74-95	[50]
PVDF/PVP/ZnO–SG	~62- 85	[79]

* Abbreviations: PSf = polysulfone; MWCNT = multi-walled carbon nanotubes; MMT = montmorillonite; mMMT = modified montmorillonite; PVDF = polyvinylidene fluoride; PVP = polyvinylpyrrolidone; ZnO–SG = zinc oxide–sol–gel composite; CA = cellulose acetate; CES = calcined eggshell.

Table 3 Variation of permeation flux from pore network and continuum models and from the experimental data

Filler loading (wt.%)	Experimental J_{exp} (10^{-4} m s^{-1})	Pore network model J_{PMN} (10^{-4} m s^{-1})	Continuum models (analytical approaches) J_{cal} (10^{-4} m s^{-1})		
			Hagen–Poiseuille model	Carman–Kozney model	Osmotic pressure model
5	8.169	7.414	0.232	1.32	5.48
10	9.436	7.842	0.075	0.011	0.0429
15	9.218	7.699	5.79	3.79	13.6
20	9.731	8.031	3.99	3.16	9.93
AARE%		15.03	73.13	77.53	20.7

Note: J_{exp}, J_{PMN}, and J_{cal} represent the experimentally measured permeation flux, the flux predicted by the pore network model, and the flux calculated from the continuum models, respectively.

and experimental data. The study compared the performance and provided deep insight into their strengths and limitations. To ensure a fair comparison, continuum and pore network models were assessed under identical operating conditions, which encompassed fluid properties, membrane thickness and applied pressure.

The results are also plotted for different CES loading (Fig. 5(a)). The comparison showed that the pore network model exhibited the lowest deviation from the experimental data, achieving an AARE of 15.03%. The AARE% calculated for the pore network model was also lower than for the continuum models. The superior performance of the pore network model was due to the structural effects of the porous media including pore size distributions, porosity, and tortuosity. The other models rely only on average values of these properties. The impact of the structural effects on the pressure distribution within the membrane can be observed in Fig. 5(b). It indicated that the pressure changes with different pore sizes of the

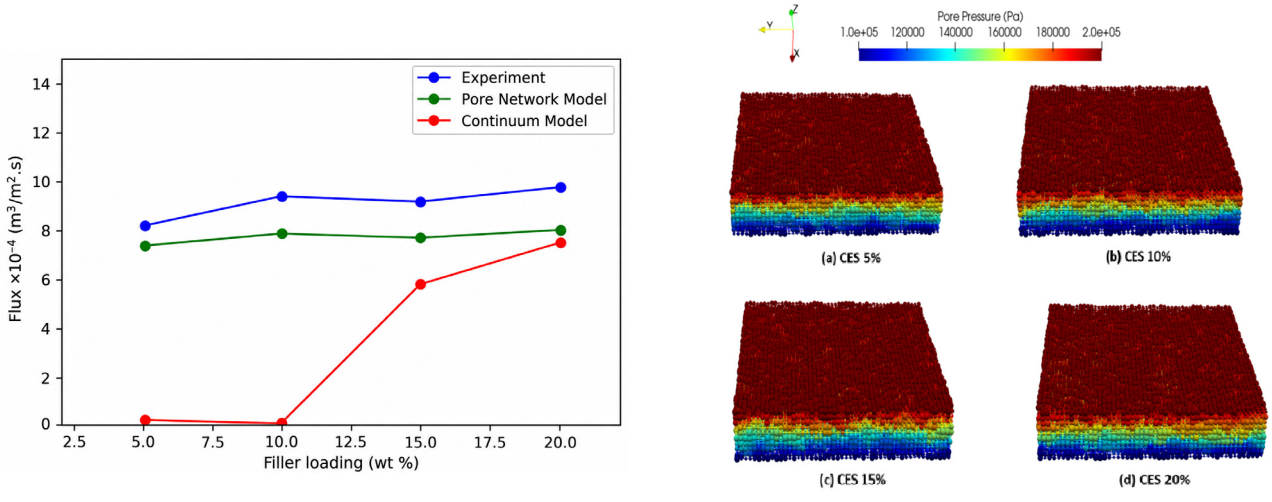

(a) (b)

Fig. 5 Hagen–Poiseuille model: (a) Comparison with experimental data; (b) Pressure distribution for different CES loading in MMMs

membranes at varying filler loading. This reveals that the pore size distribution and other structural properties of the membrane have a significant impact on the transport properties of MMMs.

Table 3 further summarizes the differences between the continuum models used in this study. The findings indicated that Hagen–Poiseuille model exhibited the lowest deviation from the empirical data. The present study revealed that the order of deviation, as determined by the AARE%, is in ascending order: the osmotic pressure model, the Hagen–Poiseuille model and the Carman–Kozeny model. However, there are major discrepancies between the computed data of the continuum model and the experimental results, prompting the need for a better model. Overall, the pore network model provided more accurate results than the continuum based model for predicting the performance of MMMs. It is important to note that the pore network modeling approach only utilized Hagen–Poiseuille model for obtaining permeation flux. Its accuracy and efficiency in osmotic pressure model and Carman–Kozeny model will be utilized in future studies to predict performance of MMMs. Future research can concentrate on enhancing the utilization of pore network model to decrease the computational time, while maintaining the structural heterogeneities of the membrane microstructure.

6 Conclusion

The present work deals with the synthesis of asymmetric MMMs at various CES filler loadings (0–20 wt.%) in CA matrix for the treatment of Cr(VI) in wastewater. The synthesized CES and MMMs were characterized by different techniques. The focus of this systematic study was to check the potential of different CES loadings on morphology and permeability of MMMs. The addition of CES led to increase in porosity and interconnectivity in MMMs shown by SEM images. The TGA analysis revealed an improvement in thermal stability with the addition of CES, with the CA/CES-15% blend exhibiting the highest degradation temperature value of 380 °C. The membranes were evaluated using a dead-end filtration assembly at 2 bar feed pressure. The permeation water flux of the MMMs increased with the increasing CES loading. The maximum permeation flux and Cr(VI) rejection of 3503 ± 32 L m^{-2} h^{-1} and 60.5 ± 80 wt.% were respectively obtained at 20 wt.% filler loading.

A comparative analysis *via* modeling approach was performed to predict the performance of the synthesized membranes. The results obtained from pore network models, continuum models and experimental data were compared and analyzed. It was found that the Hagen–Poiseuille model predicted using pore network modeling technique, presented lowest AARE% i.e. 15.03% from the experimental data. The pore network model accounted for the structural effects of the porous media, showed good capability to capture the complex and heterogeneous nature of the porous media. This resulted in more accurate predictions than the other continuum models. The study highlighted the need for further research to optimize the use of the pore network model to reduce computational time, while securing the microstructure heterogeneities of the membranes. Overall, the findings of this study have importance in design and modeling of MMMs for Cr(VI) removal and analogy-based treatment for other industrial effluents.

Acknowledgements

The authors highly acknowledge Higher Education Commission (HEC), Pakistan for the research grant under NRPU Project # 15591. Note of thanks for the collaborating universities, Novatex 2471 membrane support Freudenberg Filtration Technologies SE & Co. KG Germany and Shamim Irshad High Performance Computing Center (SIHPCC), UET Lahore, Pakistan for providing computational resources for pore networking modeling studies.

References

[1] Mbareck, C., Nguyen, Q. T., Alaoui, O. T., Barillier, D. "Elaboration, characterization and application of polysulfone and polyacrylic acid blends as ultrafiltration membranes for removal of some heavy metals from water", Journal of Hazardous Materials, 171(1–3), pp. 93–101, 2009. https://doi.org/10.1016/j.jhazmat.2009.05.123

[2] Sathya, K., Nagarajan, K., Carlin Geor Malar, G., Rajalakshmi, S., Raja Lakshmi, P. "A comprehensive review on comparison among effluent treatment methods and modern methods of treatment of industrial wastewater effluent from different sources", Applied Water Science, 12(4),70, 2022. https://doi.org/10.1007/s13201-022-01594-7

[3] Saleh, T. A. "Protocols for synthesis of nanomaterials, polymers, and green materials as adsorbents for water treatment technologies", Environmental Technology & Innovation, 24, 101821, 2021. https://doi.org/10.1016/j.eti.2021.101821

[4] Ahmad, F., Lau, K. K., Lock, S. S. M., Rafiq, S., Khan, A. U., Lee, M. "Hollow fiber membrane model for gas separation: Process simulation, experimental validation and module characteristics study", Journal of Industrial and Engineering Chemistry, 21, pp. 1246–1257, 2015. https://doi.org/10.1016/j.jiec.2014.05.041

[5] Jamil, A., Ching, O. P., Shariff, A. B. M. "Current status and future prospect of polymer-layered silicate mixed-matrix membranes for CO_2/CH_4 separation", Chemical Engineering & Technology, 39(8), pp. 1393–1405, 2016.
https://doi.org/10.1002/ceat.201500395

[6] Ismail, N. H., Salleh, W. N. W., Ismail, A. F., Hasbullah, H., Yusof, N., Aziz, F., Jaafar, J. "Hydrophilic polymer-based membrane for oily wastewater treatment: A review", Separation and Purification Technology, 233, 116007, 2020.
https://doi.org/10.1016/j.seppur.2019.116007

[7] Alshahrani, A., Alharbi, A., Alnasser, S., Almihdar, M., Alsuhybani, M., AlOtaibi, B. "Enhanced heavy metals removal by a novel carbon nanotubes buckypaper membrane containing a mixture of two biopolymers: Chitosan and i-carrageenan", Separation and Purification Technology, 276, 119300, 2021.
https://doi.org/10.1016/j.seppur.2021.119300

[8] Bhatti, H. T., Ahmad, N. M., Khan Niazi, M. B., Alvi, U. R., Azeem, …,Khan, A. U. "Graphene oxide-PES-based mixed matrix membranes for controllable antibacterial activity against salmonella typhi and water treatment", International Journal of Polymer Science, 2018(1), 7842148, 2018.
https://doi.org/10.1155/2018/7842148

[9] Rafiq, S., Man, Z., Maulud, A., Muhammad, N., Maitra, S. "Separation of CO_2 from CH_4 using polysulfone/polyimide silica nanocomposite membranes", Separation and Purification Technology, 90, pp. 162–172, 2012.
https://doi.org/10.1016/j.seppur.2012.02.031

[10] Saqib, S., Rafiq, S., Muhammad, N., Khan, A. L., Mukhtar, A., Ullah, S., Nawaz, M. H., Jamil, F., Zhang, C., Ashokkumar, V. "Sustainable mixed matrix membranes containing porphyrin and polysulfone polymer for acid gas separations", Journal of Hazardous Materials, 411, 125155, 2021.
https://doi.org/10.1016/j.jhazmat.2021.125155

[11] Ali, S., Rehman, S. A. U., Shah, I. A., Farid, M. U., An, A. K., Huang, H. "Efficient removal of zinc from water and wastewater effluents by hydroxylated and carboxylated carbon nanotube membranes: Behaviors and mechanisms of dynamic filtration", Journal of Hazardous Materials, 365, pp. 64–73, 2019.
https://doi.org/10.1016/j.jhazmat.2018.10.089

[12] Santhosh, C., Velmurugan, V., Jacob, G., Jeong, S. K., Grace, A. N., Bhatnagar, A. "Role of nanomaterials in water treatment applications: A review", Chemical Engineering Journal, 306, pp. 1116–1137, 2016.
https://doi.org/10.1016/j.cej.2016.08.053

[13] Teow, Y. H., Mohammad, A. W. "New generation nanomaterials for water desalination: A review", Desalination, 451, pp. 2–17, 2019.
https://doi.org/10.1016/j.desal.2017.11.041

[14] Qadir, D., Mukhtar, H., Keong, L. K. "Mixed matrix membranes for water purification applications", Separation & Purification Reviews, 46(1), pp. 62–80, 2017.
https://doi.org/10.1080/15422119.2016.1196460

[15] Tariq, A., Khurram, A. R., Rafiq, S., Iqbal, T., Jamil, A., …, Zaman, S. U. "Functionalized organic filler based integrated membranes for environmental remediation", Chemosphere, 303, 135073, 2022.
https://doi.org/10.1016/j.chemosphere.2022.135073

[16] Vinoba, M., Bhagiyalakshmi, M., Alqaheem, Y., Alomair, A. A., Pérez,A., Rana, P. Recent progress of fillers in mixed matrix membranes for CO2 separation: A review, Separation and Purification Technology, 188, pp. 431–450, 2017.
https://doi.org/10.1016/j.seppur.2017.07.051

[17] Saif-ur-Rehman, S. Rafiq, N. Muhammad, F. Rehman, M. Irfan, …, Show, P. L. "Surface tuning of silica by deep eutectic solvent to synthesize biomass derived based membranes for gas separation to enhance the circular bioeconomy", Fuel, 310, 122355, 2022.
https://doi.org/10.1016/j.fuel.2021.122355

[18] Khurram, A. R., Rafiq, S., Tariq, A., Jamil, A., Iqbal, T., …, Asif, S. "Environmental remediation through various composite membranes moieties: Performances and thermomechanical properties", Chemosphere, 309, 136613, 2022.
https://doi.org/10.1016/j.chemosphere.2022.136613

[19] Niazi, M. B. K., Jahan, Z., Ahmed, A., Rafiq, S., Jamil, F., Gregersen, Ø. W. "Effect of Zn-Cyclen mimic enzyme on mechanical, thermal and swelling properties of cellulose nanocrystals/PVA nanocomposite membranes", Journal of Polymers and the Environment, 28(7), pp. 1921–1933, 2020.
https://doi.org/10.1007/s10924-020-01737-4

[20] Saljoughi, E., Mohammadi, T. "Cellulose acetate (CA)/polyvinylpyrrolidone (PVP) blend asymmetric membranes: Preparation, morphology and performance", Desalination, 249(2), pp. 850–854, 2009.
https://doi.org/10.1016/j.desal.2008.12.066

[21] Rafiq, S., Man, Z., Maulud, A., Muhammad, N., Maitra, S. "Effect of varying solvents compositions on morphology and gas permeation properties on membranes blends for CO_2 separation from natural gas", Journal of Membrane Science, 378(1–2), pp. 444–452, 2011.
https://doi.org/10.1016/j.memsci.2011.05.025

[22] Rafiq, S., Man, Z., Maitra, S., Maulud, A., Ahmad, F., Muhammad, N. "Preparation of asymmetric polysulfone/polyimide blended membranes for CO_2 separation", Korean Journal of Chemical Engineering, 28(10), pp. 2050–2056, 2011.
https://doi.org/10.1007/s11814-011-0053-1

[23] Shaulsky, E., Karanikola, V., Straub, A. P., Deshmukh, A., Zucker, I., Elimelech, M. "Asymmetric membranes for membrane distillation and thermo-osmotic energy conversion", Desalination, 452, pp. 141–148, 2019.
https://doi.org/10.1016/j.desal.2018.11.005

[24] Yang, H.-C., Xie, Y., Hou, J., Cheetham, A. K., Chen, V., Darling, S. B. "Janus Membranes: Creating Asymmetry for Energy Efficiency", Advanced Materials, 30(43), 1801495, 2018.
https://doi.org/10.1002/adma.201801495

[25] Tian, Y., Wu, M., Liu, R., Li, Y., Wang, D., Tan, J., Wu, R., Huang, Y. "Electrospun membrane of cellulose acetate for heavy metal ion adsorption in water treatment", Carbohydrate Polymers, 83(2), pp. 743–748, 2011.
https://doi.org/10.1016/j.carbpol.2010.08.054

[26] Jamil, A., Zulfiqar, M., Arshad, U., Mahmood, S., Iqbal, T., Rafiq, S., Iqbal, M. Z. "Development and performance evaluation of cellulose acetate-bentonite mixed matrix membranes for CO_2 separation", Advances in Polymer Technology, 2020(1), 8855577, 2020.
https://doi.org/10.1155/2020/8855577

[27] Abu-Zurayk, R., Alnairat, N., Khalaf, A., Ibrahim, A. A., Halaweh, G. "Cellulose Acetate Membranes: Fouling Types and Antifouling Strategies – A Brief Review", Processes, 11(2), 489, 2023.
https://doi.org/10.3390/pr11020489

[28] Haddada, R., Ferjani, E., Roudesli, M. S., Deratani, A. "Properties of cellulose acetate nanofiltration membranes. Application to brackish water desalination", Desalination, 167, pp. 403–409, 2004.
https://doi.org/10.1016/j.desal.2004.06.154

[29] Sofi, H. S., Akram, T., Shabir, N., Vasita, R., Jadhav, A. H., Sheikh, F. A. "Regenerated cellulose nanofibers from cellulose acetate: Incorporating hydroxyapatite (HAp) and silver (Ag) nanoparticles (NPs), as a scaffold for tissue engineering applications", Materials Science and Engineering: C, 118, 111547, 2021.
https://doi.org/10.1016/j.msec.2020.111547

[30] Elsayed, M. T., Hassan, A. A., Abdelaal, S. A., Taher, M. M., Ahmed, M. k., Shoueir, K. R. "Morphological, antibacterial, and cell attachment of cellulose acetate nanofibers containing modified hydroxyapatite for wound healing utilizations", Journal of Materials Research and Technology, 9(6), pp. 13927–13936, 2020.
https://doi.org/10.1016/j.jmrt.2020.09.094

[31] Pandele, A. M., Neacsu, P., Cimpean, A., Staras, A. I., Miculescu, F., Iordache, A., Voicu, S. I., Thakur, V. K., Toader, O. D. "Cellulose acetate membranes functionalized with resveratrol by covalent immobilization for improved osseointegration", Applied Surface Science, 438, pp. 2–13, 2018.
https://doi.org/10.1016/j.apsusc.2017.11.102

[32] Ahmad, A., Waheed, S., Khan, S. M., Shafiq, M., Farooq, M., Sanaullah, K., Jamil, T. "Effect of silica on the properties of cellulose acetate/polyethylene glycol membranes for reverse osmosis", Desalination, 355, pp. 1–10, 2015.
https://doi.org/10.1016/j.desal.2014.10.004

[33] Jamshaid, A., Hamid, A., Muhammad, N., Naseer, A., Ghauri, M., Iqbal, J., Rafiq, S., Shah, N. S. "Cellulose-based Materials for the Removal of Heavy Metals from Wastewater–An Overview", ChemBioEng Reviews, 4(4), pp. 240–256, 2017.
https://doi.org/10.1002/cben.201700002

[34] Abu-Dalo, M. A., Al-Rosan, S. A., Albiss, B. A. "Photocatalytic Degradation of Methylene Blue Using Polymeric Membranes Based on Cellulose Acetate Impregnated with ZnO Nanostructures", Polymers, 13(19), 3451, 2021.
https://doi.org/10.3390/polym13193451

[35] Vatanpour, V., Yuksekdag, A., Ağtaş, M., Mehrabi, M., Salehi, E., Castro-Muñoz, R., Koyuncu, I. "Zeolitic imidazolate framework (ZIF-8) modified cellulose acetate NF membranes for potential water treatment application", Carbohydrate Polymers, 299, 120230, 2023.
https://doi.org/10.1016/j.carbpol.2022.120230

[36] Saeed, M.,Rafiq, M., Bergersen, L. H., Deng, L. "Tailoring of water swollen PVA membrane for hosting carriers in CO_2 facilitated transport membranes", Separation and Purification Technology, 179, pp. 550–560, 2017.
https://doi.org/10.1016/j.seppur.2017.02.022

[37] Ur Rehman, R., Rafiq, S., Muhammad, N., Khan, A. L., Ur Rehman, A., TingTing, L., Saeed, M., Jamil, F., Ghauri, M., Gu, X. "Development of ethanolamine-based ionic liquid membranes for efficient CO_2/CH_4 separation", Journal of Applied Polymer Science, 134(44), 45395, 2017.
https://doi.org/10.1002/app.45395

[38] Kadhom, M., Al-Furaiji, M., Salih, S., Al-Obaidi, M. A., Abdullah, G. H., Albayati, N. "A review on UiO-66 applications in membrane-based water treatment processes", Journal of Water Process Engineering, 51, 103402, 2023.
https://doi.org/10.1016/j.jwpe.2022.103402

[39] Qadir, D., Mukhtar, H., Keong, L. K. "Synthesis and characterization of polyethersulfone/carbon molecular sieve based mixed matrix membranes for water treatment applications", Procedia Engineering, 148, pp. 588–593, 2016.
https://doi.org/10.1016/j.proeng.2016.06.517

[40] Naseer,A., Hamid, A., Ghauri, M., Nasrullah ,A., Iqbal, J., Shah, N. S., Rafiq, S., Irfan, M., Muhammad, N. "Lignin/alginate/hydroxyapatite composite beads for the efficient removal of copper and nickel ions from aqueous solutions", Desalination and Water Treatment, 184, pp. 199–213, 2020.
https://doi.org/10.5004/dwt.2020.25356

[41] Zaman, S. U., Saif-ur-Rehman, Zaman, M. K. U., Arshad, A., Rafiq, S., …, Sadiq, M. T. "Biocompatibility performance evaluation of high flux hydrophilic CO3Ap/HAP/PSF composite membranes for hemodialysis application", Artificial Organs, 45(8), pp. E265–E279, 2021.
https://doi.org/10.1111/aor.13937

[42] You, P., Kamarudin, S. K., Masdar, M. S. "Improved performance of sulfonated polyimide composite membranes with rice husk ash as a bio-filler for application in direct methanol fuel cells", International Journal of Hydrogen Energy, 44(3), pp. 1857–1866, 2019.
https://doi.org/10.1016/j.ijhydene.2018.11.166

[43] Zaman, S. U., Zaman, M. K. U., Irfan, M., Rafiq, S., Irfan, M., Muhammad, N., Saif-ur-Rehman, Wajeeh, S., Naz, G. "Biocompatible chicken bone extracted dahllite/hydroxyapatite/collagen filler based polysulfone membrane for dialysis", The International Journal of Artificial Organs, 45(1), pp. 14–26, 2022.
https://doi.org/10.1177/0391398821994119

[44] Sowińska-Baranowska, A., Maciejewska, M. "Potential Utilization of Ground Eggshells as a Biofiller for Natural Rubber Biocomposites", Materials, 16(8), 2988, 2023.
https://doi.org/10.3390/ma16082988

[45] Habte, L., Shiferaw, N., Mulatu, D., Thenepalli,T., Chilakala, R., Ahn, J. W. "Synthesis of nano-calcium oxide from waste eggshell by sol-gel method", Sustainability, 11(11), 3196, 2019.
https://doi.org/10.3390/su11113196

[46] Lumlong, S., Wanapan, S., Khamsri, B., Pungpo, P. "Effect of Eggshell as a Filler on Rubber Composite Properties", In: The 8th Thailand-Japan International Academic Conference, 2016, pp. 1–7.

[47] Khan, R. Z., Khurram, M. S., Rafiq, S., Inayat, A., Hussain, A., Bokhari, A., Aslam, M., Jamil, F. "Efficient wastewater treatment by utilizing biomass derived adsorbent: A comprehensive study to prove its commercial viability", [preprint] Research Square, 07 February 2022.
https://doi.org/10.21203/rs.3.rs-1225214/v1

[48] Sunardi, S., Ariawan, D., Surojo, E., Prabowo, A. R., Akbar, H. I., Cao, B., Carvalho, H. "Assessment of eggshell-based material as a green-composite filler: Project milestones and future potential as an engineering material", Journal of the Mechanical Behavior of Materials, 32(1), 20220269, 2023.
https://doi.org/10.1515/jmbm-2022-0269

[49] Park, H. J., Jeong, S. W., Yang, J. K., Kim, B. G., Lee, S. M. "Removal of heavy metals using waste eggshell", Journal of Environmental Sciences, 19(12), pp. 1436–1441, 2007.
https://doi.org/10.1016/S1001-0742(07)60234-4

[50] Jacob, L., Joseph, S., Varghese, L. A. "Polysulfone/MMT Mixed Matrix Membranes for Hexavalent Chromium Removal from Wastewater", Arabian Journal for Science and Engineering, 45(9), pp. 7611–7620, 2020.
https://doi.org/10.1007/s13369-020-04711-3

[51] Li, R., Liu, L., Yang, F. "Removal of aqueous Hg(II) and Cr(VI) using phytic acid doped polyaniline/cellulose acetate composite membrane", Journal of Hazardous Materials, 280, pp. 20–30, 2014.
https://doi.org/10.1016/j.jhazmat.2014.07.052

[52] Pettinato, M.,Chakraborty, M., Arafat, H. A., Calabro, V. "Eggshell: a green adsorbent for heavy metal removal in an MBR system", Ecotoxicology and Environmental Safety, 121, pp. 57–62, 2015.
https://doi.org/10.1016/j.ecoenv.2015.05.046

[53] Aslam, M., Ahmad, R., Yasin, M., Khan, A. L., Shahid, M. K., Hossain, S., Khan, Z., Jamil, F., Rafiq, S., Bilad, M. R. "Anaerobic membrane bioreactors for biohydrogen production: Recent developments, challenges and perspectives", Bioresource Technology, 269, pp. 452–464, 2018.
https://doi.org/10.1016/j.biortech.2018.08.050

[54] Jamil, A., Ching, O. P., Iqbal, T, Rafiq, S., Zia-ul-Haq, M., Shahid, M. Z., Mubashir, M., Manickam, S., Show, P. L. "Development of an extended model for the permeation of environmentally hazardous CO_2 gas across asymmetric hollow fiber composite membranes", Journal of Hazardous Materials, 417, 126000, 2021.
https://doi.org/10.1016/j.jhazmat.2021.126000

[55] Rajinder, P. "Permeation models for mixed matrix membranes", Journal of Colloid and Interface Science, 317(1), pp. 191–198, 2008.
https://doi.org/10.1016/j.jcis.2007.09.032

[56] Saqib, S., Rafiq, S., Muhammad, N., Khan, A. L., Mukhtar, A., Mellon, N. B., Man, Z., Ullah, S., Al-Sehemi, A. G., Jamil, F. "Influence of interfacial layer parameters on gas transport properties through modeling approach in MWCNTs based mixed matrix composite membranes", Chemical Engineering Science, 218, 115543, 2020.
https://doi.org/10.1016/j.ces.2020.115543

[57] Mukhtar, A., Saqib, S., Safdar, F., Hameed, A., Rafiq, S., …, Merican, Z. M. A. "Experimental and comparative theoretical study of thermal conductivity of MWCNTs-kapok seed oil-based nanofluid", International Communications in Heat and Mass Transfer, 110, 104402, 2020.
https://doi.org/10.1016/j.icheatmasstransfer.2019.104402

[58] Hashemifard, S. A., Ismail, A. F., Matsuura, T. "Prediction of gas permeability in mixed matrix membranes using theoretical models", Journal of Membrane Science, 347(1–2), pp. 53–61, 2010.
https://doi.org/10.1016/j.memsci.2009.10.005

[59] Khan, Z. A., Agnaou, M., Sadeghi, M. A., Elkamel, A., Gostick, J. T. "Pore Network Modelling of Galvanostatic Discharge Behaviour of Lithium-Ion Battery Cathodes", Journal of The Electrochemical Society, 168(7), 070534, 2021.
https://doi.org/10.1149/1945-7111/ac120c

[60] van Gorp, R., van der Heijden, M., Amin Sadeghi, M., Gostick, J., Forner-Cuenca, A. "Bottom-up design of porous electrodes by combining a genetic algorithm and a pore network model", Chemical Engineering Journal, 455, 139947, 2023.
https://doi.org/10.1016/j.cej.2022.139947

[61] Khan, Z. A., Salaberri, P. A. G., Heenan, T. M. M., Jervis, R., Shearing, P. R., Brett, D., Elkamel, A., Gostick, J. T. "Probing the Structure-Performance Relationship of Lithium-Ion Battery Cathodes Using Pore-Networks Extracted from Three-Phase Tomograms", Journal of Electrochemical Society, 167(4), 040528, 2020.
https://doi.org/10.1149/1945-7111/ab7bd8

[62] Sadeghnejad, S., Gostick, J. "Multiscale Reconstruction of Vuggy Carbonates by Pore-Network Modeling and Image-Based Technique", SPE Journal, 25(01), pp. 253–267, 2020.
https://doi.org/10.2118/198902-PA

[63] McKague, M., Fathiannasab, H., Agnaou, M., Sadeghi, M. A., Gostick, J. "Extending pore network models to include electrical double layer effects in micropores for studying capacitive deionization", Desalination, 535, 115784, 2022.
https://doi.org/10.1016/j.desal.2022.115784

[64] Sadeghi, M. A., Aghighi, M., Barralet, J., Gostick, J. T. "Pore network modeling of reaction-diffusion in hierarchical porous particles: The effects of microstructure", Chemical Engineering Journal, 330, pp. 1002–1011, 2017.
https://doi.org/10.1016/j.cej.2017.07.139

[65] Zhang, D., Zhang, X., Guo, H., Lin, D., Meegoda, J. N., Hu, L. "An anisotropic pore-network model to estimate the shale gas permeability", Scientific Reports, 11(1), 7902, 2021.
https://doi.org/10.1038/s41598-021-86829-4

[66] Ali, M., Aslam, M., Khan, A., Gilani, M. A., Khan, A. L. "Mixed matrix membranes incorporated with sonication-assisted ZIF-8 nanofillers for hazardous wastewater treatment", Environmental Science and Pollution Research, 26(35), pp. 35913–35923, 2019.
https://doi.org/10.1007/s11356-019-06698-3

[67] Gostick, J., Aghighi, M., Hinebaugh, J., Tranter, T., Hoeh, M. A., Day, H. "OpenPNM: A Pore Network Modeling Package", Computing in Science & Engineering, 18(4), pp. 60–74, 2016.
https://doi.org/10.1109/MCSE.2016.49

[68] Ang, W., Mohammad, A. W. "Mathematical modeling of membrane operations for water treatment", In: Basile, A., Cassano, A., Rastogi, N. K. (eds.) Advances in Membrane Technologies for Water Treatment, Woodhead Publishing, 2015, pp. 379–407. ISBN 978-1-78242-121-4
https://doi.org/10.1016/B978-1-78242-121-4.00012-5

[69] Genne, I., Kuypers, S., Leysen, R. "Effect of the addition of ZrO2 to polysulfone based UF membranes", Journal of Membrane Science, 113(2), pp. 343–350, 1996.
https://doi.org/10.1016/0376-7388(95)00132-8

[70] Seader, J. D., Henley, E. J., Roper, D. K. "Separation process principles", Wiley New York, 1998. ISBN 978-0-470-48183-7

[71] Li, W., Xing, W., Xu, N. "Modeling of relationship between water permeability and microstructure parameters of ceramic membranes", Desalination, 192(1–3), pp. 340–345, 2006. https://doi.org/10.1016/j.desal.2005.07.042

[72] Lawal, D. U. "Desalination using air gap membrane distillation", MSc Thesis, King Fahd University of Petroleum and Minerals, Saudi Arabia, 2014.

[73] Van der Bruggen, B., Vandecasteele, C., Van Gestel,T., Doyen, W., Leysen, R. "A review of pressure-driven membrane processes in wastewater treatment and drinking water production", Environmental Progress, 22(1), pp. 46–56, 2003. https://doi.org/10.1002/ep.670220116

[74] Arthanareeswaran, G., Thanikaivelan, P., Srinivasn, K., Mohan, D., Rajendran, M. "Synthesis, characterization and thermal studies on cellulose acetate membranes with additive", European Polymer Journal, 40(9), pp. 2153–2159, 2004. https://doi.org/10.1016/j.eurpolymj.2004.04.024

[75] Abou-Zeid, N., Waly, A., Kandile, A., Rushdy, A., El-Sheikh, M., Ibrahim, H. M. "Preparation, characterization and antibacterial properties of cyanoethylchitosan/cellulose acetate polymer blended films", Carbohydrate Polymers, 84(1), pp. 223–230, 2011. https://doi.org/10.1016/j.carbpol.2010.11.026

[76] Ren, X., Zhao, C., Du, S., Wang, T., Luan, Z., Wang, J., Hou, D. "Fabrication of asymmetric poly (m-phenylene isophthalamide) nanofiltration membrane for chromium (VI) removal", Journal of Environmental Sciences, 22(9), pp. 1335–1341, 2010. https://doi.org/10.1016/S1001-0742(09)60259-X

[77] Mukherjee, R., De, S. "Adsorptive removal of phenolic compounds using cellulose acetate phthalate–alumina nanoparticle mixed matrix membrane", Journal of Hazardous Materials, 265, pp. 8–19, 2014. https://doi.org/10.1016/j.jhazmat.2013.11.012

[78] Shah, P., Murthy, C. N. " Studies on the porosity control of MWCNT/polysulfone composite membrane and its effect on metal removal", Journal of Membrane Science, 437, pp. 90–98, 2013. https://doi.org/10.1016/j.memsci.2013.02.042

[79] Chabane, M., Melkaoui, C., Dahmani, B. " Preparation and Characterization of Matrix Hybrid Membranes Polyvinylidene Fluoride/Polyvinylpyrrolidone/Silica Gel/Zinc Oxide for Cr(VI) Removal from Water", Advances in Materials Science and Engineering, 44(5), pp. 311–318, 2020. https://doi.org/10.18280/acsm.440502